ARCHIVES OF ELECTRICAL ENGINEERING VOL. 67(4), pp. 869–884 (2018)

DOI 10.24425/aee.2018.124746

Design of protective and stabilizing controllers: a study with considering natural events

EHSAN GANJI[1], MEHDI MAHDAVIAN[2], HOSEIN SHIRZADI[3]

[1] *Acecr Institute of higher Education*
Kermanshah, Iran

[2] *Department of Electrical Engineering, Naein Branch, Islamic Azad University*
Naein, Iran

[3] *Department of Electrical Engineering, Kermanshah Branch, Islamic Azad University*
Kermanshah, Iran
e-mail: Mr.ehsanganji@gmail.com

(Received: 19.02.2018, revised: 10.09.2018)

Abstract: In renewable systems, there may be conditions that can be either network error or power transmission line and environmental conditions such as when the wind speed is unbalanced and the wind turbine is connected to the grid. In this case, the control system is not damaged and will remain stable in the power transmission system. Voltage stability studies on an independent wind turbine at fault time and after fixing the error is one of the topics that can strengthen the future of independent collections. At the time of the fault, the network current increases dramatically, resulting in a higher voltage drop. Hence the talk of fast voltage recovery during error and after fixing the error and protection of rotor and grid side converters against the fault current and also protection against rising DC voltage (which sharply increases during error) is highly regarded. So, several improvements have been made to the construction of a doubly-fed induction generator (DFIG) turbine such as: a) error detection system, b) DC link protection, c) crow bar circuit, d) block of the rotor and stator side converters, e) injecting reactive power during error, f) nonlinear control design for turbine blades, g) tuning and harmonization of controllers used to keep up the power quality and to stabilize the system output voltage in the power grid. First, the dynamic models of a wind turbine, gearbox, and DFIG are presented. Then the controllers are modeled. The results of the simulation have been validated in MATLAB/Simulink.

Key words: wind turbine, error detection system, output stability of the turbine, crow bar circuit, tuning PI controllers, power quality

1. Introduction

In the modern world, the environmental laws of most countries have always contributed to the use of renewable energy, especially for energy production. Among these renewable energies,

wind energy is highly regarded as a potential source of power generation. The advancement of technology in wind energy conversion equipment (WECS), such as electric machines and power converters, leads to the use of variable speed turbines (VSWTs). The analysis and compensation of voltage imbalances in a DFIG, using prediction of rotor flow control under unbalanced loads and the compensation method, have been used to balance the stator output voltage. It is also implemented based on a flow control prediction (PCC) approach and it is developed in rotor flow control [1, 2].

In the wind turbine systems, the problem of compensating for harmonics, appearing with an increase in wind power and unbalanced load, is still significant and a solution for the problem should be found. The use of algebraic algorithms is an interesting solution in the design of a resonant controller [4]. In [5], a motion sensor and the algorithm for control and stability of the wind turbine to cut frequency problems in the control system were proposed.

The input of this system was designed with nonlinear controls, which ultimately resulted in more power and high reliability in the output. To consider high reliability in the wind turbine system at the time of an error in the network or transmission line, the fault ride-through (FRT) method was used to track most of the power, it will be optimally implemented in the output voltage setting at the fault time [6].

In independent systems the use of an asynchronous controller can bring a good result. This system increases the low voltage ride-through (LVRT) capability within the uncertainty framework and the use of nonlinear controllers to control the high-pressure voltage in wind turbine generators [7]. In [8] the modeling of a real machine show that using the vector control method and stator flux control has created the ability to generate power in a doubly-fed induction machine (DFIM).

The use of non-linear and dynamic controllers in controlling the flux of the rotor ability aims to control the wind turbine in precarious conditions. In addition, coordinating a fuzzy controller with a high degree of slip mode can accurately trace the power point [9]. In the discussion it had been proved that using the effects of the crowbar circuit for short-term faults in wind systems, control, and evaluation under various error conditions, has improved the low voltage switching ability (LVRT) [10].

In the wind turbines, the use of a voltage control system and one (LVRT) controller, both nonlinear, can cut the speed of the turbine response, and it also reduces oscillation of the rotor current, the electromagnetic torque, and the voltage across the gradient generator's voltages [11]. In [12], we can see the effect of the error switch using the crowbar circuit resistance that after simulation shows, the effect of different resistance in the rotor current and active and reactive power. Designing and using closed-loop control algorithms for a power factor in the DFIM turbines can show significant computational loads [13].

Basically, to protect the power converters during voltage drop, the crowbar system is used to prevent reactive power absorption of the grid [14]. A limited cycle control for current and torque using a switching table can optimize and stabilize the inverter output. Creating this limited cycle control is possible with magnetic field control [15].

In the converter, devices and three-phase systems use a significant performance controller that can control the induction torque through sequential triggers to a given flux relation in transient and continuous conditions [16]. Direct control methods can be evaluated and can control the instantaneous active power of converters by the switch modes.

This strategy is deeply focused on two factors of total power and harmonic components [17]. In [18] a three-phase pulse modulation for direct power control is used based on flow estimation. The result of this controller is a dynamic behavior and stable VF-DPC. In induction machines, to control the instantaneous torque response and the flux of the voltage converter and a sensitive sensor control method, active and reactive power are created to track resources from numerical controllers [19]. In electric machines, the initial flux on the rotor side does not affect the reactive power and the stator modulus curve. As well as very much attention has been paid to the increasing number of voltage components using vector modulation in direct power control [20, 21]. In variable mode systems, topics and strategies such as isolation, tracking transactions, and the lack of sensitivity to variable parameters used for the problem of slider mode in the converters are researched [22].

In general, wind problems and slipping problems can create instabilities in wind turbines which in front of nonlinear and PI controllers can increase system efficiency [23]. To eliminate power failure errors and synchronize the entire system, it can be used for the slider and control of the rotor voltage. As well as, the use of (LUT) DPC, followed by the increase in transient performance and the stable state of the harmonic spectrum [24]. In [25], the Author shows the reduction of tracking errors and energy quality disturbances using simultaneous PI controllers, the integral sliding mode control (ISMC), and the particle swarm algorithm with high reliability. The nonlinear PI controllers and high-order slip mode can be useful to increase productivity and to increase energy production [26]. Using a medium-voltage current-source converter (MV CSC) in high voltage systems for high reliability can increase the safety of the system and check the performance configuration in different conditions [27].

In a modeling wind turbine system, the use of computer programs can offer sustainability in the dynamic performance of the system and a set of disturbances and changes in wind speed [28]. So, several improvements have been made to the construction of the DFIG turbine such as: a) error detection system, b) DC link protection, c) crow bar circuit, d) block of the rotor and stator side converters, e) injecting reactive power during error, f) nonlinear control design for turbine blades, g) tuning and harmonization of controllers used to keep up the power quality and to stabilize the system output voltage in the power grid.

2. The description of the studied context

The study is based on a DFIG wind turbine (Fig. 1).

2.1. The turbine model

In standard DFIG modeling, we have the following relationships [2]:

$$P_a = 0.5\rho\pi R^2 V_w^3 C_p(\lambda, \beta). \tag{1}$$

From the above relation for C_P a non-linear relationship is as follows:

$$C_P(\lambda) = \beta_0 + \beta_1\lambda + \beta_2\lambda^2 + \beta_3\lambda^3 + \beta_4\lambda^4 + \beta_5\lambda^5, \tag{2}$$

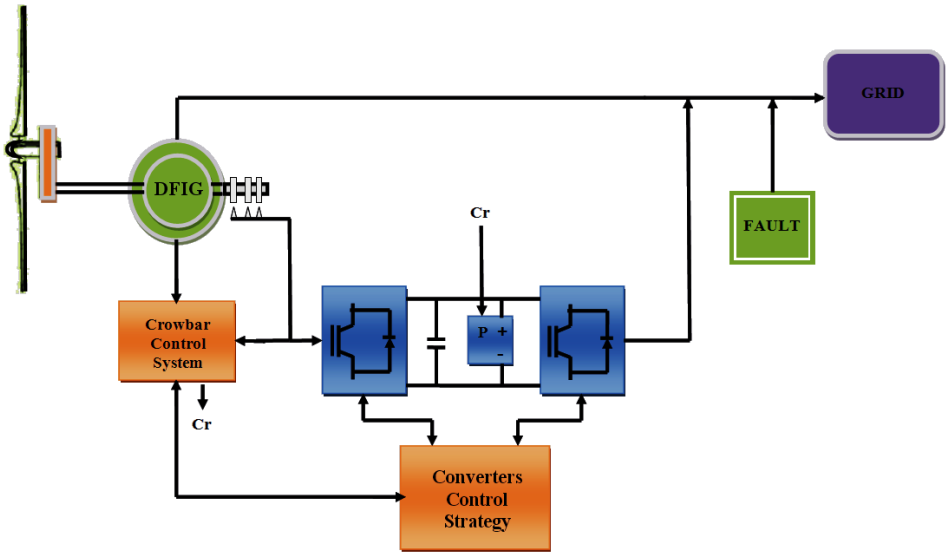

Fig. 1. The structure of the studied context

where:

$$\lambda = \frac{R\omega_t}{V_w}. \tag{3}$$

That

$$C_T(\lambda, \beta) = \frac{C_p(\lambda, \beta)}{\lambda}. \tag{4}$$

For the airspeed we have the following model:

$$V_{\text{ride}} = V_{nt} + \frac{(c - 45)\,(V_{st} - V_{nt})}{115 - 70}. \tag{5}$$

Following the above relationships, we can get the system current from the park's relationship and with the use of the nonlinear PI controllers; we can define the reference relationships of the currents as follows:

$$\begin{cases} I_{sd\_\text{ref}} = 0 \\ I_{sq\_\text{ref}} = \dfrac{T_{em}\_T_{em\_\text{PMSG\_ref}}}{p\phi_m} \end{cases}. \tag{6}$$

We define the electromagnetic torque by considering the maximum power point and with the equations of current obtained from the park's relationship and other elements, we can define the relationships DQ voltage rotor and stator as follows:

$$T_{em\_\text{turbin\_ref}} = \frac{\rho\pi R^5 C_{p\,\max}}{2\lambda_{\text{opt}}^3}\Omega^2, \tag{7}$$

$$\begin{cases} v_{ds} = -R_s i_{ds} - \omega_s \psi_{qs} + \dfrac{\mathrm{d}\psi_{ds}}{\mathrm{d}t} \\ v_{qs} = -R_s i_{qs} - \omega_s \psi_{ds} + \dfrac{\mathrm{d}\psi_{qs}}{\mathrm{d}t} \\ v_{dr} = -R_r i_{dr} - \omega_r \psi_{qr} + \dfrac{\mathrm{d}\psi_{dr}}{\mathrm{d}t} \\ v_{qr} = -R_r i_{qr} - \omega_r \psi_{dr} + \dfrac{\mathrm{d}\psi_{qr}}{\mathrm{d}t} \end{cases} . \tag{8}$$

3. Design of system strategies

Fig. 1 shows the architecture of the proposed study bed, where the controller diagrams are depicted. We often present here the strategy and proposed systems in the form of an orbital diagram. However, the other control strategies mentioned in the abstract, which are not seen in the diagram in Fig. 1, are explained in the discussion below.

3.1. DFIG model

In the modeling of this generator system, a two-axis model is used in the block of the diagram and its relation is as follows (Fig. 2):

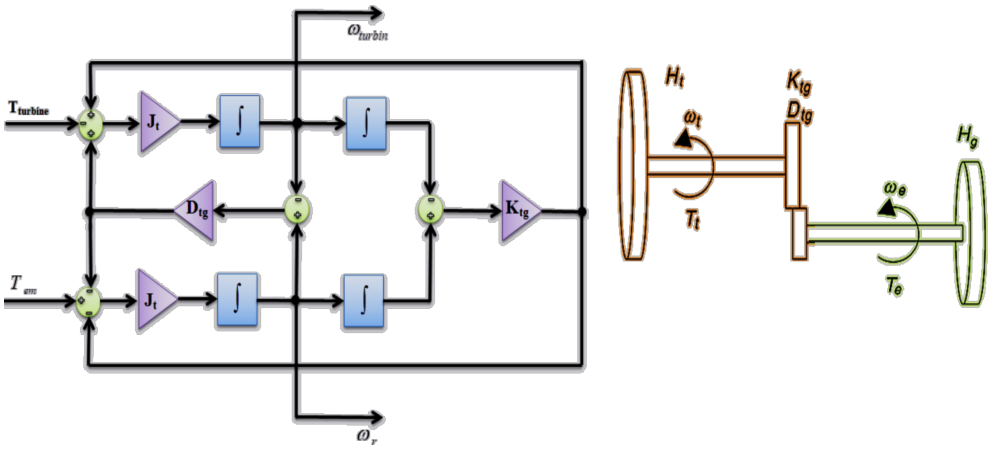

(a) (b)

Fig. 2. Two-axis model (a) and its block diagram (b)

This model is as follows:

$$\frac{\omega_r(s)}{T_{em}(s)} = \frac{1}{(J_t + J_g)s} \frac{J_t s^2 + D_{tg} s + K_{tg}}{\dfrac{J_t J_g}{J_t + J_g} s^2 + D_{tg} s + K_{tg}} . \tag{9}$$

3.2. Creation of torque control system

In this design, we use the linear and nonlinear relationships as well as feedback cycles from the wind speed system and the feedback sent from the system output, we were able to improve the standard active power control. In the image below you can see the dynamic diagram (Fig. 3).

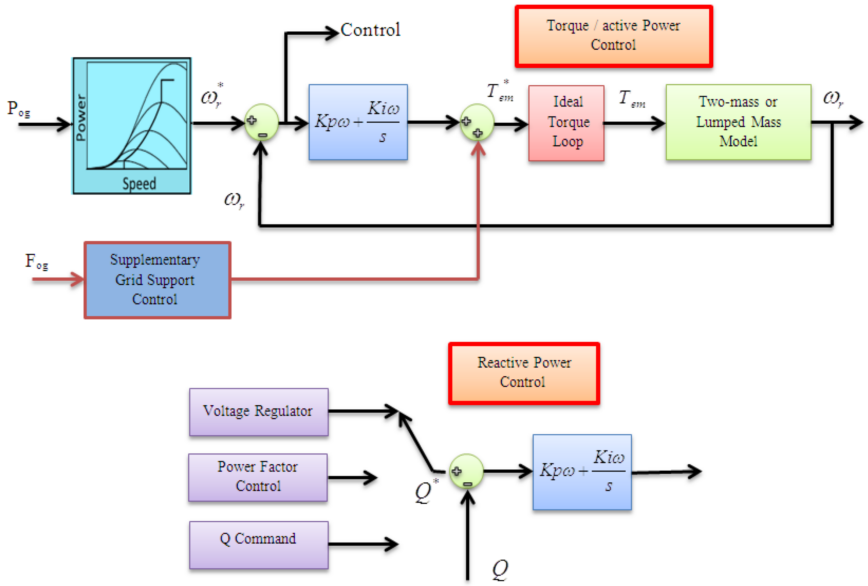

Fig. 3. Diagram of torque control

3.3. Crowbar system

In this system, when the output of the network voltage is lower than 0.8, then the error detection system operates and generates signals to control the system's protection. The following figure shows the modeling of this system (Fig. 4).

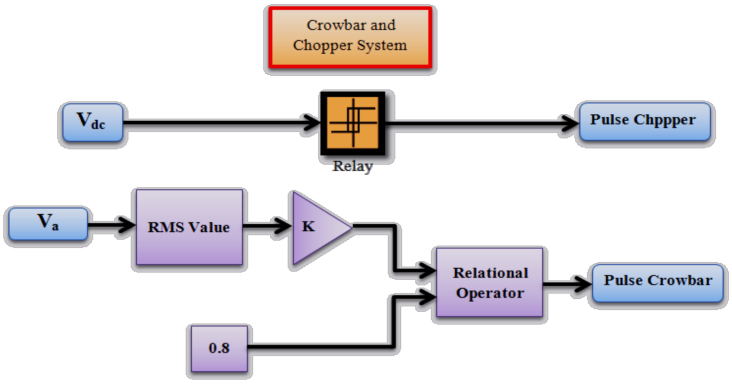

Fig. 4. Crowbar and chopper system diagram

3.3.1. Protective circuit in crowbar system

With respect to the ideal power system standards, at the time of the lack of voltage, the DFIG should not be disconnected from the grid. For this reason, at the time of the error or deficiency of the rotor, the induction motor is connected to a resistor through a rectifier circuit, which in fact, converts the DFIG into a wiring rotor generator. It is necessary to note that when the resistance resides in the circuit, an error occurs. This control is via a key with which it is cached (the key command comes from the error detection system, (explained in the previous section). The circuit is as follows (Fig. 5):

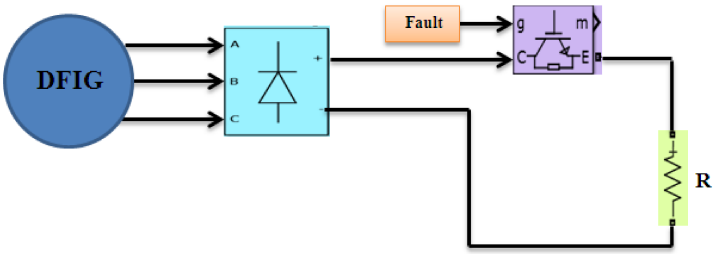

Fig. 5. Protective circuit of the crowbar system

3.3.2. Protective circuit for DC link

To control the DC link, the control system designed in such a way that when the DC link voltage is higher than the specified value, it sends a command to key series with the resistance. Immediately the parallel capacitor with resistance is placed in the circuit, which protects the DC link (Fig. 6).

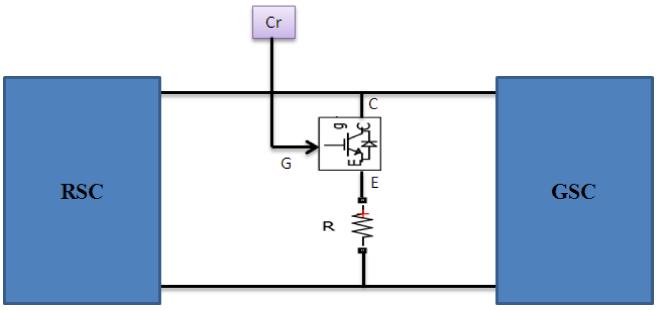

Fig. 6. DC link chopper circuit

3.3.3. The control of the blade pitch

First, we consider the definitions and the conditions of continuity for wind disturbances. We define $f_1 = x_1$, $f_2 = \dot{x}_1$ and $z_3 = \varphi(x, f)$; thus, we obtain the following equations:

$$\begin{cases} \dot{f}_1 = f_2 + \gamma\beta_0 \\ \dot{f}_2 = f_3 + b_0 u + \gamma(\beta_0, t) \\ \dot{f}_3 = \Psi(x, \beta_0, t) \end{cases} . \tag{10}$$

With following $\widetilde{f_1} = f_1 - \hat{f}_1$, we obtain a linear TSPl:

$$\begin{cases} \dot{\hat{f}}_1 = \hat{f}_2 + k_{01}\widetilde{f_1} + \hat{\gamma}\beta_0 \\ \dot{\hat{f}}_2 = \hat{f}_3 + b_0 u + k_{02}\widetilde{f} + \hat{\gamma}(\beta_0, t) \\ \dot{\hat{f}}_3 = k_{03}\widetilde{f} \end{cases} . \tag{11}$$

With following $\hat{f}_1 (i = 1, 2, 3)$ and $\widetilde{f_1}$ a fault is obtained for f_1. If k_{0i} is the parameter coefficient, than:

$$[k_{01} \;\; k_{02} \;\; k_{03}] = [3\gamma_0 \;\; 3\gamma_0^2 \;\; 3\gamma_0^3], \tag{12}$$

in which the γ_0 online controller is based on the bandwidth of the system and is configurable.

Here, for the wind speed and its nonlinear control, we have the following relation:

$$\begin{cases} \dot{\hat{f}}_1 = \hat{f}_2 + k_{01}\widetilde{f_1}(\gamma_0, \beta_0) \\ \dot{\hat{f}}_2 = \hat{f}_3 + b_0 u + k_{02} fal\,(\widetilde{f_1}, \gamma_0, \beta_0, h) \\ \dot{\hat{f}}_3 = k_{03} fal\,(\widetilde{f_1}, \gamma_0, \beta_0, h) \end{cases} , \tag{13}$$

$$faltn\,(x, \gamma, h) = \begin{cases} \dfrac{\gamma^2}{h^{(1-\sigma)}} x & |x| \le h \\ \text{sign}\,(x)\gamma^2 |x|^{\sigma} & |x| > h \end{cases} . \tag{14}$$

Given the relationships and disputes, we write the input as follows:

$$u = \frac{1}{b_0} ki \left(v - \hat{\Psi}(x)\right), \tag{15}$$

also

$$v = \left(k_p + \frac{k_i}{s}\right)(\omega_r^* - x_1 - \beta_0) . \tag{16}$$

Eventually, the nonlinear control is obtained as below:

$$u = \frac{1}{b_0}\left(k_p + \frac{k_i}{s}\right)(\omega_r^* - x_1 - \beta_0) - \frac{1}{b_0}\hat{\Psi}(x, \alpha_0). \tag{17}$$

The design of the turbine blade control system is shown in the Figure 7, where the required value is obtained from Table 1 and equations and also the advantage of this controller is its intelligence and accurateness.

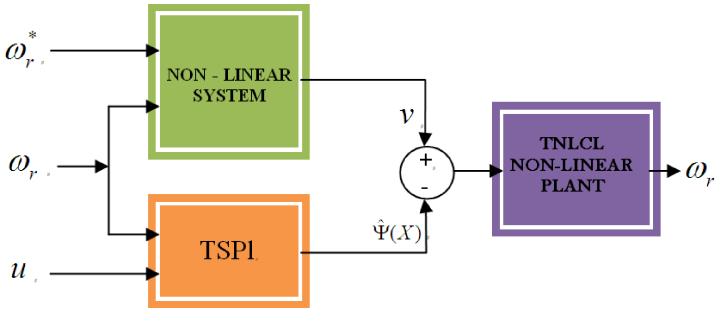

Fig. 7. The proposed nonlinear PI controller

Table 1. The nonlinear controller and the TNLCL parameters

Parameters	Value
TLC/NL-PI proportional gain ($1/s^2$)	8.3
TLC/NL-PI integral gain (1/s), k_i	1.23
TSPl equivalent input gain ($^\circ s^3$/rad), b_0	1.09
TSPl nonlinear coefficient (rad/s), h	0.094
TSPl observer bandwidth, γ_0	24
TSPl estimation gain (1/s), $k\,\gamma_1$	1.8×10^3
TSPl estimation gain ($1/s^2$), $k\,\gamma_2$	2.9×10^3
TSPl estimation gain ($1/s^3$), $k\,\gamma_3$	4.6×10^5

3.4. Converters control strategy

3.4.1. Rotor-side converter control

Here the main purpose of the control is to get the maximum power from the wind speed under the mode factor (mainly wind speed). At each electromagnetic torque; the speed of the DFIG rotor is controlled. The reference torque obtained by a speed control loop and the angle required to send the network voltage using a closed loop phase (PLL). The torque value is tracked with maximum power loop. During turbulence, the turbine system must remain stable, which requires accurate controllers. However, in a DFIG, both active power and reactive power in the stator can be independently controlled. It can be used to offer voltage regulation or reactive power support. Here, the q-axis rotor value is used to control the reactive power.

3.4.2. Grid-side converter control

The DC link voltage is controlled by active power control in the GSC section with the d-axis flow components. In addition to reactive power control in RSC, the reactive power output in the GSC can be controlled independently through the components of the q-axis. In addition, in the GSC section, the voltage parameters are fixed at the DQ axes, but the current parameters check the stability of the system in different modes.

3.4.3. Smart blocks strategy for grid side converter

The RSC turbine section of the DFIG in the reference frame DQ injects independently active and reactive power and the GSC control system has been used to regulate the DC link voltage between the two converters. To prevent damage to parts of turbine converters at the time of the error or the lack of voltage that occurs due to the high current, the passage of both converters was blocked. To do this, a switch that works in all the pulse modes that come from the control of the converters sends to the output, at error time, a command from the error detection section; this key switches and sends the zero pulse to the output, which causes inactivation of the converters. The following diagram is for the two parts of the rotor and the network, which we modeled by adding a pulse error.

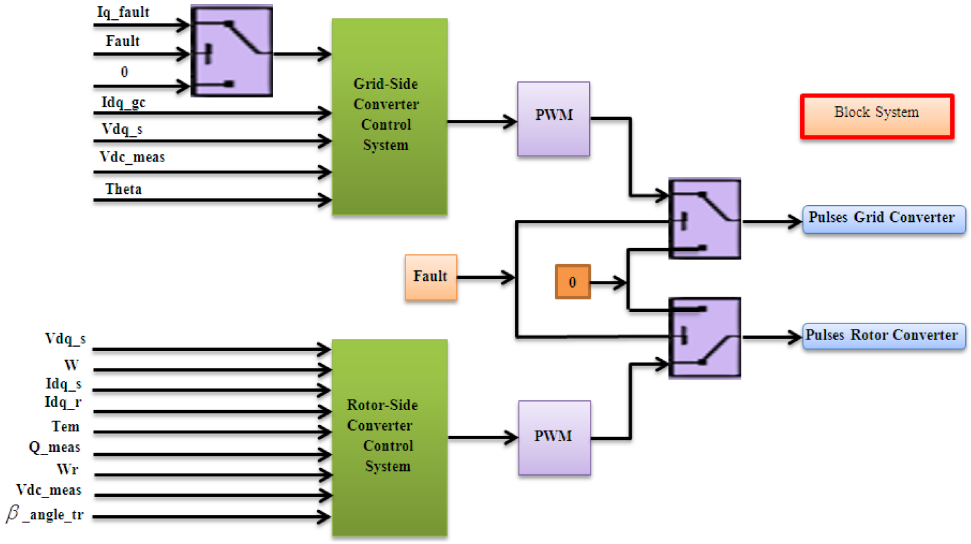

Fig. 8. Diagram of blocking converters

3.5. Design of rotor flow control during fault

After the error is detected, the reactive power injection control system enters the circuit and injects reactive power into the system, which is visible in the diagram below. The system voltage is related to the injection reactive power. Therefore, the reference voltage compared with the measured voltage and their difference after crossing the PI controller as reactive power reference

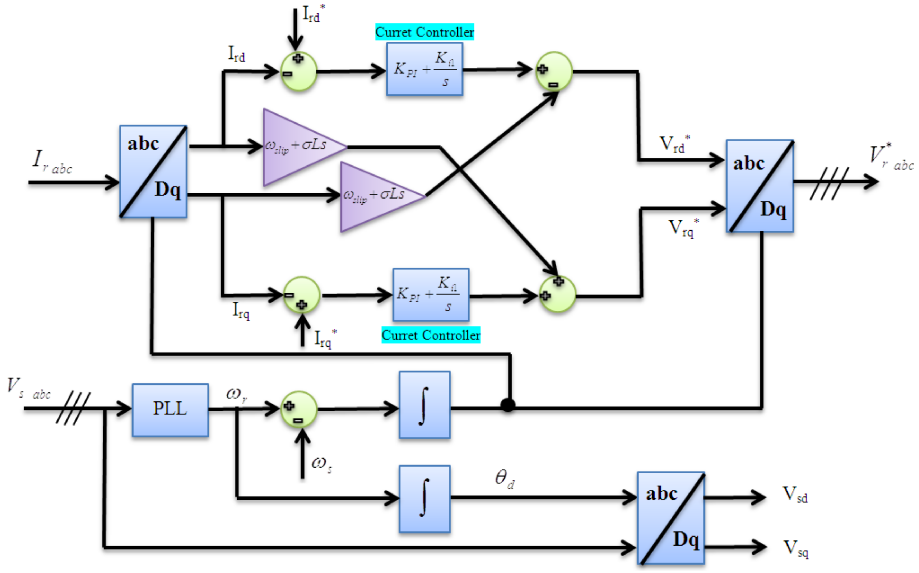

Fig. 9. Block diagram of rotor current control

enters the network controller. This function controls the voltage error and returns it to the reference value because the reactive power is sufficiently injected into the system.

Feeding the block diagram shown in the figure above is as follows:

$$\frac{I_{rd}(s)}{V_{rd}(s)} = \frac{1}{R_r + s\sigma L_r}, \tag{18}$$

$$V_{rq} = R_r i_{rq} + \sigma L_r \frac{\mathrm{d}}{\mathrm{d}t} i_{rq} + \omega_{\text{slip}} \sigma L_r i_{rd} + \omega_{\text{slip}} \frac{L_m}{L_s} \lambda_{sd}. \tag{19}$$

The fit integral controller (PI) performed for two loops and is easily simplified for the transfer functions and the design proposed for a band of desired width and phase margin.

4. The simulation results

In this section, we want to present the simulation results of the proposed control strategies for wind turbines with a double-fed induction generator. In this experiment, which lasts for 10

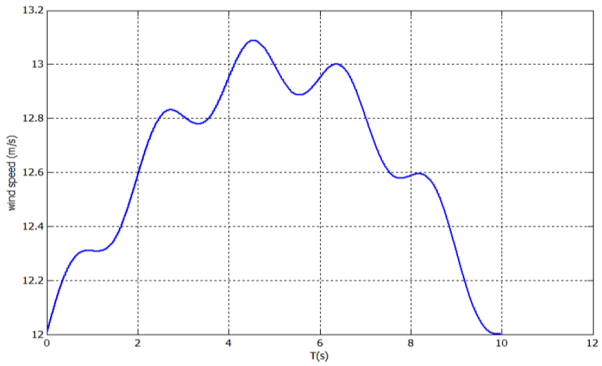

(a)

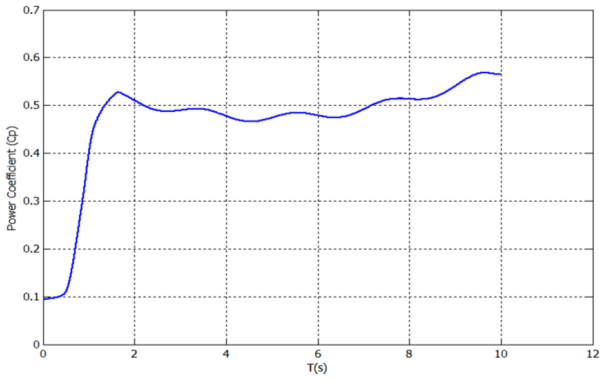

(b)

Fig. 10. (a) wind speed, (b) power quality factor

seconds, the network error occurs within 1 to 2 seconds and, in addition, a the disruptions in wind speed from the start to the end of the experiment always happens.

In the above figures, you can see the wind speed and the power quality coefficient. In this study, the standard speed 12 m/s for the turbine has been considered. Here, the accuracy and power of the controllers used have been able to achieve a power quality coefficient of 0.56, which is a significant amount compared with many other papers.

In the strategies of this research, the non-linear control of turbine blades at the time of the disorder begins to change the angle that after passing a certain amount continues to half the blades angle. Also in the reverse change state again from a certain amount that was considered, it starts to change the blade angle to zero. In Figures 11(b) and (c), you can see the signal of the crossover fault detection and the circuit chopper at the time of the disruption.

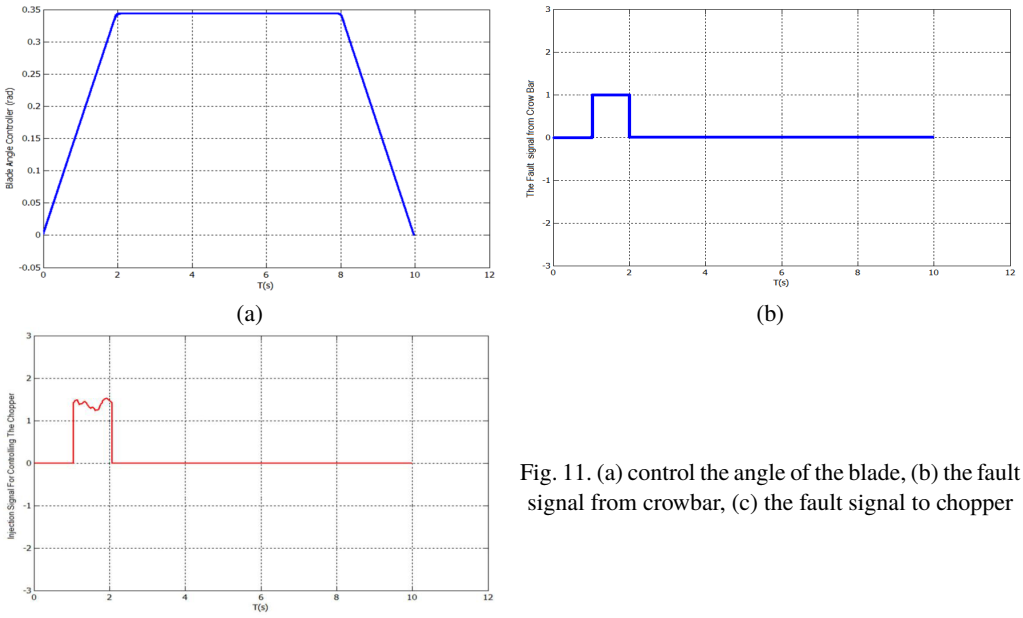

Fig. 11. (a) control the angle of the blade, (b) the fault signal from crowbar, (c) the fault signal to chopper

In Fig. 12, sections (a) and (b), you can see the output shapes of the rotor and stator converters. In section (b), at the time of the disruption, it disconnected the output curve in the stator converter. This breakdown function is monitored by the controller. In sections (c) and (d), you can see the outputs of the DQ axis, these outputs are fully controlled and will remain unchanged under disturbances.

In Fig. 13 you can see the three-phase current output in the various bus-lines of the transmission line. A disruption has occurred in the BT575 bus but using the reactive power injection strategy, dumper, and breaker, the disorder is fully controlled and next compensated by the buses.

In Fig. 14, the three-phase outputs of the voltage are visible on different buses and clearly, show the effect of control strategies.

Fig. 15 shows active and reactive power outputs where in section (a) you can see that the system output power is controlled at 1.5 MW. In this section, the disorders were fully controlled

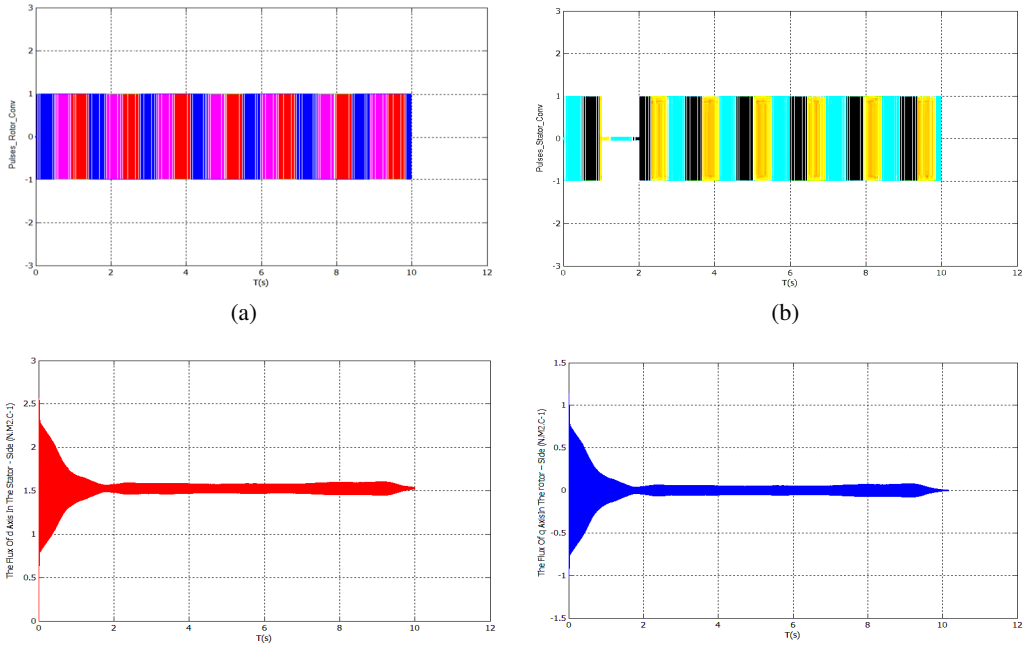

(a) (b)

(c) (d)

Fig. 12. (a) rotor-side converter pulses, (b) stator-side converter pulses, (c) the flux of d-axis the stator-side, (d) the flux of q-axis the rotor-side

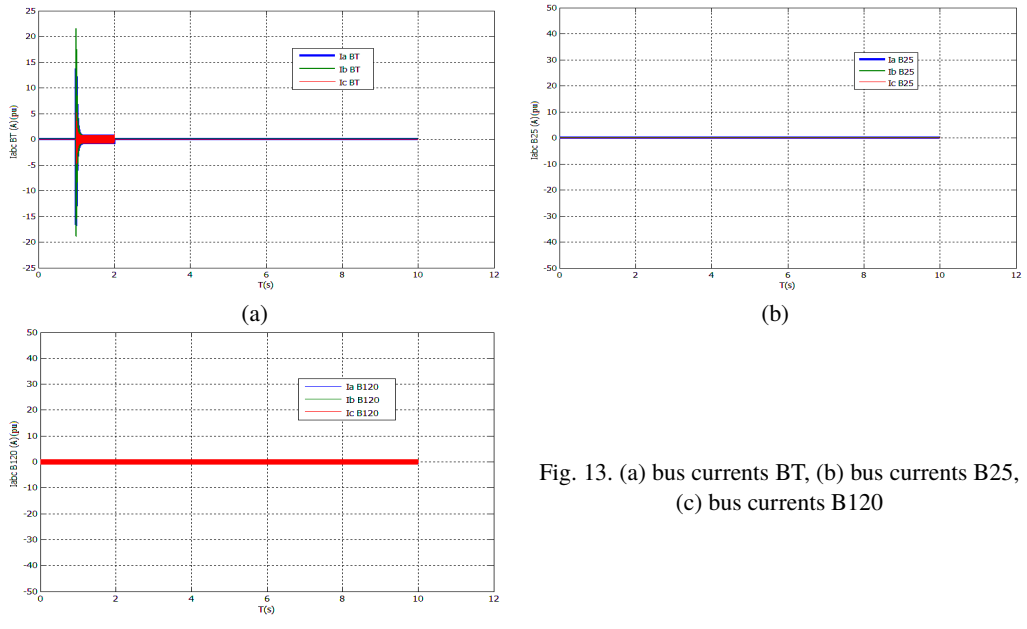

(a) (b)

(c)

Fig. 13. (a) bus currents BT, (b) bus currents B25, (c) bus currents B120

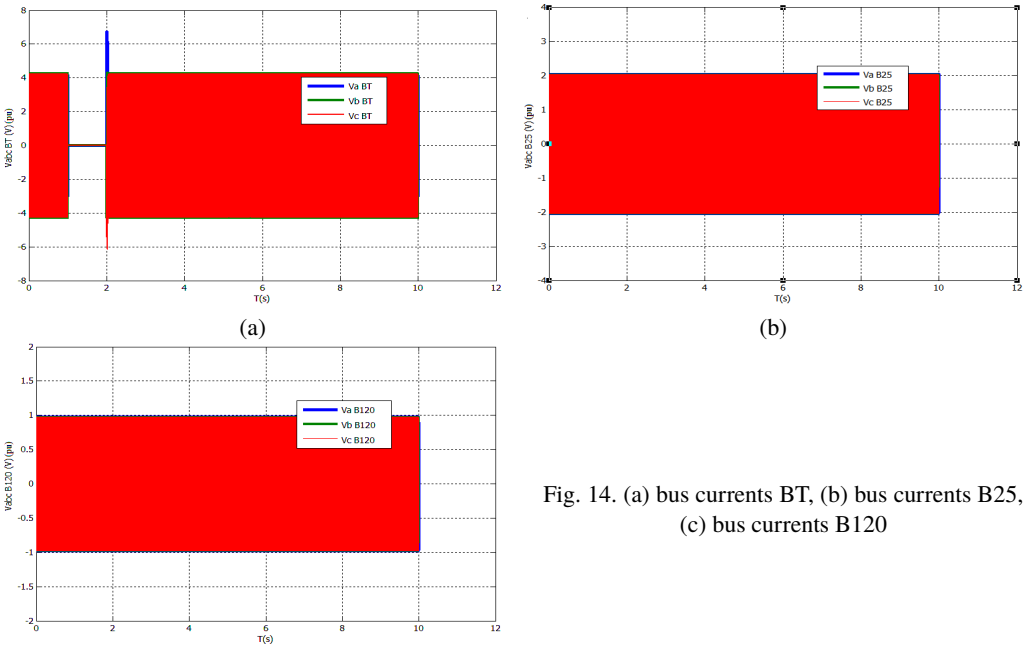

Fig. 14. (a) bus currents BT, (b) bus currents B25, (c) bus currents B120

and did not affect the active power amount. In section (b), you can see the reactive power that has changed during the disruption in the transmission line to compensate and control the disorder.

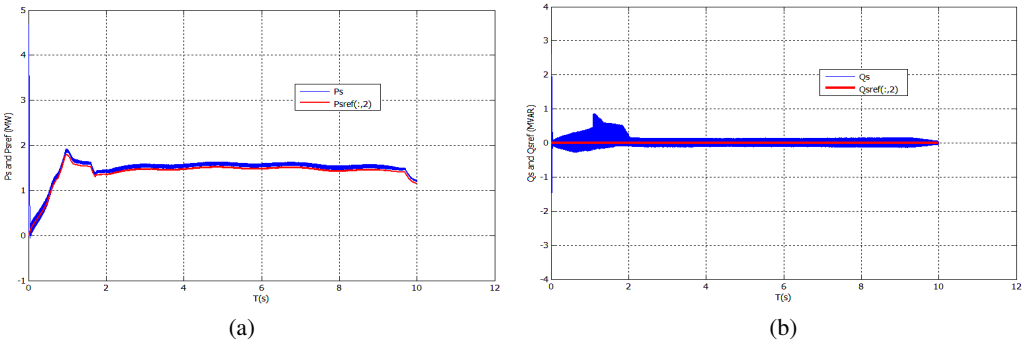

Fig. 15. (a) measured active power and reference power, (b) measured reactive power and reference power

5. Conclusions

Because of the unpredictable nature of the wind and error occur possibility; the concept of fixing the output voltage of the system has been researched. We controlled and verified the wind turbine output voltage varies for a specific type of wind turbine system for different wind

speed values. Hence, the result should consider solutions to stabilize the voltage at different wind velocities and different error states.

The analysis of simulated results showed that a set of measures taken to stabilize DFIG voltage and protection included the use of an error detection system, speed controller system, crowbar protection system, chopper DC link and reactive power compensation which eventually lead to the right answer for a proper DFIG construction. After eliminating the error, the voltage returns time set at a time set by different standards and compliance with the requirements of the network.

In the turbine blade control system, a precise output was obtained and we saw that the controller corrected the angle of the blades without any distortion. Also, in the fault detection and crowbar system, the signals quickly entered the protection system. It's easy to say that these two systems control 90 percent of the setup error protection. In the end, we were able to control the output of the system at 1.5 MW and put it into the power grid and also control the transmission line error. The strategies designed in this research are designed simply for use in exploitation projects and do not cost much to implement.

References

[1] Phan V.T., Logenthiran T., Woo W.L., Atkinson D., Pickert V., *Analysis and compensation of voltage unbalance of a DFIG using predictive rotor current control*, International Journal of Electrical Power & Energy Systems, vol. 29, no. 75, pp. 8–18 (2016).

[2] Abdeddaim S., Betka A., *Optimal tracking and robust power control of the DFIG wind turbine*, Electrical Power and Energy Systems, vol. 49, pp. 234–242 (2013).

[3] Abdelkafi A., Masmoudi A., Krichen L., *Experimental investigation on the performance of an autonomous wind energy conversion system*, International Journal of Electrical Power & Energy Systems, vol. 44, no. 1, pp. 581–590 (2013).

[4] Chen W.L., Jiang B.Y., *Harmonic Suppression and Performance Improvement for a Small-scale Grid-tied Wind Turbine Using Proportional–Resonant Controllers. Electric Power Components and Systems*, vol. 43, no. 8–10, pp. 970–981 (2015).

[5] Qiao W., Zhou W., Aller J.M., Harley R.G., *Wind speed estimation based sensorless output maximization control for a wind turbine driving a DFIG*, IEEE transactions on power electronics, vol. 23, no. 3, pp. 1156–1169 (2008).

[6] Kyaw M.M., Ramachandaramurthy V.K., *Fault ride through and voltage regulation for grid connected wind turbine*, Renewable Energy, vol. 36, no. 1, pp. 206–215 (2011).

[7] Hossain M.J., Pota H.R., Ramos R.A., *Robust STATCOM control for the stabilisation of fixed-speed wind turbines during low voltages*, Renewable Energy, vol. 36, no. 11, pp. 2897–2905 (2011).

[8] Tapia A., Tapia G., Ostolaza J.X., Saenz J.R., *Modeling and control of a wind turbine driven doubly fed induction generator*, IEEE Transactions on energy conversion, vol. 18, no. 2, pp. 194–204 (2003).

[9] Ganji E., Mahdavian M.A., *Controlling Method of DFIG-Based Wind Turbine for Stability Improvement of Power Delivery to the Power Grid*, Journal of Electrical Systems, vol. 12, no. 3, pp. 591–611 (2016).

[10] Shi L., Chen N., Lu Q., *Dynamic characteristic analysis of doubly-fed induction generator low voltage ride-through*, Energy Procedia, vol. 16, pp. 1526–1534 (2012).

[11] Rahimi M., Parniani M., *Grid-fault ride-through analysis and control of wind turbines with doubly fed induction generators*, Electric Power Systems Research, vol. 80, no. 2, pp. 184–195 (2010).

[12] Noureldeen O., *Behavior of DFIG wind turbines with crowbar protection under short circuit*, International Journal of Electrical and Computer Sciences IJECS, vol. 12, no. 3, pp. 32–37 (2012).

[13] Tapia G., Tapia A., Ostolaza J.X., *Two alternative modeling approaches for the evaluation of wind farm active and reactive power performances*, IEEE transactions on energy conversion, vol. 21, no. 4, pp. 909–920 (2006).

[14] Peng L., Francois B., Li Y., *Improved crowbar control strategy of DFIG based wind turbines for grid fault ride-through*, In Applied Power Electronics Conference and Exposition, APEC 2009, Twenty-Fourth Annual IEEE, vol. 15, pp. 1932–1938 (2009).

[15] Takahashi I., Noguchi T., *A new quick-response and high-efficiency control strategy of an induction motor*, IEEE Transactions on Industry applications, vol. 5, iss. IA–22, pp. 820–827 (1986).

[16] Depenbrock M., *Direct self-control (DSC) of inverter-fed induction machine*, IEEE transactions on Power Electronics, vol. 3, no. 4, pp. 420–429 (1988).

[17] Noguchi T., Tomiki H., Kondo S., Takahashi I., *Direct power control of PWM converter without power-source voltage sensors*, IEEE Transactions on Industry Applications, vol. 34, no. 3, pp. 473–479 (1998).

[18] Malinowski M., Kazmierkowski M.P., Hansen S., Blaabjerg F., Marques GD., *Virtual-flux-based direct power control of three-phase PWM rectifier*s, IEEE Transactions on industry applications, vol. 37, no. 4, pp. 1019–1027 (2001).

[19] Datta R., Ranganathan V.T., *Direct power control of grid-connected wound rotor induction machine without rotor position sensors*, IEEE Transactions on Power Electronics, vol. 16, no. 3, pp. 390–399 (2001).

[20] Xu L., Cartwright P., *Direct active and reactive power control of DFIG for wind energy generation*, IEEE Transactions on energy conversion, vol. 21, no. 3, pp. 750–758 (2006).

[21] Kazemi M.V., Yazdankhah A.S., Kojabadi H.M., *Direct power control of DFIG based on discrete space vector modulation*, Renewable Energy, vol. 35, no. 5, pp. 1033–1042 (2010).

[22] Utkin V.I., *Sliding mode control design principles and applications to electric drives*, IEEE transactions on industrial electronics, vol. 40, no. 1, pp. 23–36 (1993).

[23] Hu J., Nian H., Hu B., He Y., Zhu Z.Q., *Direct active and reactive power regulation of DFIG using sliding-mode control approach*, IEEE Transactions on Energy Conversion, vol. 25, iss. 4, pp. 1028–1039 (2010).

[24] Aboulem S., Boufounas E.M., *Optimal tracking and robust intelligent based PI power controller of the wind turbine systems*, In 2017 Intelligent Systems and Computer Vision (ISCV), pp. 1–7 (2017).

[25] Elghali S.B., Benbouzid M.E., Ahmed-Ali T., Charpentier J.F., Mekri F., *High-order sliding mode control of DFIG-based marine current turbine*, In Industrial Electronics, IECON 2008, 34th Annual Conference of IEEE 2008, vol. 10, pp. 1228–1233 (2008).

[26] Wei Q., Wu B., Xu D.D., Zargari N.R., *A New Configuration Using PWM Current Source Converters in Low-Voltage Turbine-Based Wind Energy Conversion Systems*, IEEE Journal of Emerging and Selected Topics in Power Electronics (2017).

[27] Anderson P.M., Bose A., *Stability simulation of wind turbine systems*, IEEE Transactions on Power Apparatus and Systems, vol. 3, iss. 12, pp. 3791–3795 (1983).

[28] Kundur P., Balu N.J., Lauby M.G., *Power system stability and control*, New York: McGraw-hill (1994).